Inverting reflections using full-waveform inversion with inaccurate starting models

Abdullah AlTheyab and G. T. Schuster, King Abdullah University of Science and Technology (KAUST)*

SUMMARY

We present a method for inverting seismic reflections using full-waveform inversion (FWI) with inaccurate starting models. For a layered medium, near-offset reflections (with zero angle of incidence) are unlikely to be cycle-skipped regardless of the low-wavenumber velocity error in the initial models. Therefore, we use them as a starting point for FWI, and the subsurface velocity model is then updated during the FWI iterations using reflection wavepaths from varying offsets that are not cycle-skipped.

To enhance low-wavenumber updates and accelerate the convergence, we take several passes through the non-linear Gauss-Seidel iterations, where we invert traces from a narrow range of near offsets and finally end at the far offsets. Every pass is followed by applying smoothing to the cumulative slowness update. The smoothing is strong at the early stages and relaxed at later iterations to allow for a gradual reconstruction of the subsurface model in a multiscale manner. Applications to synthetic and field data, starting from inaccurate models, show significant low-wavenumber updates and flattening of common-image gathers after many iterations.

INTRODUCTION

The goal of FWI (Tarantola, 1984; Virieux and Operto, 2009) is to infer a subsurface model by minimizing the difference between the observed and calculated data. The FWI misfit function, however, is known to be non-linear with many local minima, often caused by cycle-skipping (Gauthier et al., 1986). Therefore, local-gradient optimization algorithms often get stuck at a local minimum providing implausible subsurface models.

A set of methods have been developed to mitigate the cycle-skipping problem, while maintaining the original FWI formulation. Cycle-skipped events are excluded by filtering in different transform domains (Bunks et al., 1995; Asnaashari et al., 2012), or by evaluating the phase lag between the observed and calculated data for each event and muting cycle-skipped events (Bi and Lin, 2014). In general, such methods apply FWI in multistages. At every stage, part of the data is inverted using the objective function

$$J_i\left(\delta\mathbf{m}_i\right) = \frac{1}{2}\left\|\mathbf{W}_i \triangle\mathbf{d}\left(\mathbf{m}_i + \delta\mathbf{m}_i\right)\right\|_2^2, \quad (1)$$

where the subscript i denotes the stage number, $\triangle\mathbf{d}$ is the difference between the observed and calculated data, $\mathbf{W}_i$ is a weighting operator that excludes (by multiplication by zero) the cycle-skipped events in the data. $\mathbf{m}_i$ is the initial model at the $i-$th stage, and $\delta\mathbf{m}_i$ is the cumulative model updated to the initial model $\mathbf{m}_i$ needed to fit the data. After each stage, a new model is computed

$$\mathbf{m}_{i+1} = \mathbf{m}_i + \delta\mathbf{m}_i, \quad (2)$$

where $\mathbf{m}_{i+1}$ is the initial model for the following stage. Note that at each stage the objective function is minimized with many iterations. As the model is gradually updated, previously cycle-skipped events become uncycle-skipped and the weighting operator is updated accordingly to include new uncycle-skipped events in the next stage. Such approaches are effective for inverting transmitted waves (direct arrivals, head waves, and diving waves) which cover the shallow sections of the Earth. However, they are insufficient for updating the background velocity model using reflections below the reach of transmitted waves.

It is believed that the primary cause of FWI failure in updating the low-wavenumber components of the model is the weakness of the tomographic terms in the update kernels of FWI (Zhou et al., 2012). Therefore, several approaches for enhancing the tomographic components were proposed for reflection FWI while minimizing the difference between the observed and calculated data (Zhou et al., 2012; Xu et al., 2012; Wang et al., 2013; Brossier et al., 2013). Such approaches use scale separation between high-wavenumber and low-wavenumber components of the model where they are inverted at every iteration in separate steps: the imaging step (where the reflectors are mapped in the subsurface) and the tomography step, where the low-wavenumber updates are computed based on the data misfit function.

There are two main disadvantages to the proposed approaches. First, they are based on the single scattering assumption, and therefore higher-order scattering can not be handled accurately. In addition, the transmitted waves have to be removed from the data before inversion. The second disadvantage is that the implementations bear the additional cost of several wavefield simulations needed in the imaging and the tomography steps. To avoid the single scattering assumption and the additional costs, AlTheyab et al. (2013) proposed using Gauss-Newton optimization when inverting reflections using FWI, where low-wavenumber updates along reflection-wavepaths are naturally enhanced within the FWI iterations.

However, the success of all aforementioned solutions for updating the low-wavenumber components is limited to recovering localized mid-wavenumber anomalies when the reflectors are close to their accurate positions, which requires an accurate starting model. This raises the question whether the weakness of reflection wavepaths is the sole cause for the failure in updating the low-wavenumber components of the model.

We believe that the main problem is the coupling between the low-wavenumber components of the model to all the high-wavenumber components, as well as the contradicting updates along reflection wavepaths from different angles of incidence. To solve this problem, we propose splitting the FWI problem at each stage such that we sequentially invert a narrow-offset range of traces, starting with the short offsets and ending at the far offsets. We will refer to FWI with a narrow-

DOI http://dx.doi.org/10.1190/segam2015-5849854.1

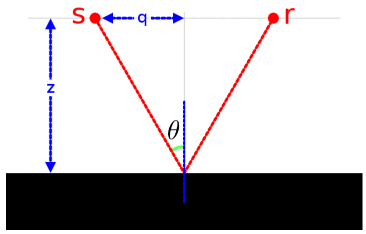

Figure 1: Geometrical configuration for a source and a receiver with a horizontal interface.

offset range as constant-offset FWI. In each constant-offset FWI, Gauss-Newton optimization is used, and the final velocity model of a constant-offset FWI is the initial model to the following constant-offset FWI. This approach is closely related to the non-linear block Gauss-Seidel iteration method with overlapping blocks (Tai, 1992; Gutiérrez et al., 2011). Here, each constant-offset FWI is naturally tuned for enhancing low-wavenumber updates along reflection wavepaths. In the following sections, we will elaborate on the coupling problem and the proposed solution to enhance the low-wavenumber updates. Later, we show the results of applying the proposed method to synthetic and field data, where low-wavenumber errors in the starting model are corrected after many stages. Finally, we comment on the generalization of the method.

THEORY

For a reflection or scattering event, there are a group of receivers along a planar surface where the travel-time gradient of the specified reflection is zero ($\nabla\tau(x,y) \approx \mathbf{0}$), which maps to stationary events in the data where the apparent velocity is zero. This is usually true for near-offset reflections from a layered medium. Such events are unlikely to be cycle-skipped during FWI for any smooth starting model. Therefore, we design the weighting operator $\mathbf{W}$ in equation 1 to only allow such uncycle-skipped event into FWI, and the windows are gradually widened to include more uncycle-skipped data as we proceed to later stages with an improved initial model. This process can be automated such that cycle-skipping is detected in an adaptive manner as in Bi and Lin (2014).

This multistage FWI with automatic detection and exclusion of cycle-skipping is extremely slow and impractical if the starting model contains significant low-wavenumber errors. That is because subsurface reflectors will be mispositioned in the early iterations, and the positioning has to be gradually corrected with a large number of iterations. To illustrate the cause of slow convergence, we consider the following scenario.

Consider a horizontally invariant two-layer model shown in Figure 1 which will give a single reflection from the deep interface between the two layers. For a homogeneous starting velocity model, the angle of incidence, for a horizontally invariant model, is related to the model wavenumber via the relation (Sirgue and Pratt, 2004)

$$k_z = 2\frac{\omega}{c}\cos\theta, \tag{3}$$

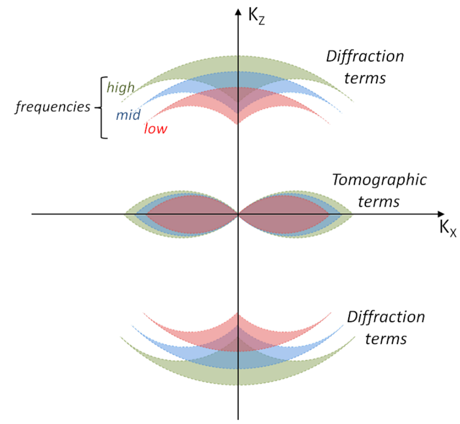

Figure 2: The wavenumber coverage from diffraction terms and tomographic (reflection transmission) terms of different frequencies.

where ω, c, and θ are, respectively, the angular frequency, the initial velocity, and the angle of incidence. When there are low-wavenumber errors in the initial velocity model, the model phase $\phi(k_z)$ will be a weighted average of the phases from different angles and frequencies that cover the same wavenumber k_z (i.e. the apparent depth of the reflector will be a weighted average of apparent depths from different angles). At the second iteration, phase delays of predicted specular events will vary depending on the angles of incidence θ. It follows, then, that there will be both positive and negative phase delays between the observed and calculated waveforms depending on the angle of incidence.

In the following FWI iterations, the mispositioned reflector will act as a secondary source for updating the low-wavenumber components of the model via reflection wavepaths. Figure 2 shows the wavenumber coverage for a model with a single reflector (see Mora (1989) for details) where the tomographic terms are related to reflection wavepaths. Even though there is little overlap between the wavenumber coverage between the diffraction terms from different frequencies and angles of incidence, the corresponding tomographic terms are completely overlapping at the small wavenumbers near the origin. This illustrates the strong coupling between the high wavenumbers (from different angles and frequencies) and the low wavenumbers reconstructed by the tomographic terms in Figure 2. Therefore, the positive and negative phase errors result in conflicting updates in the tomographic terms (i.e. the overlapping zone in Figure 2), and, consequently, negligible low-wavenumber updates from reflection residuals.

To resolve the strong coupling and the conflicting updates, the objective function in equation 1 at the $i-$th stage, is regrouped into different terms based on source-receiver offset,

$$J_i(\delta\mathbf{m}_i) = \frac{1}{2}\sum_{h}^{N}\left\|\mathbf{W}_i^h \triangle\mathbf{d}_i^h(\mathbf{m}_i+\delta\mathbf{m}_i)\right\|^2, \tag{4}$$

where the superscript h denote the offset index and N is the number of offsets bins in the data. For the model in Figure 1,

DOI http://dx.doi.org/10.1190/segam2015-5849854.1

the source-receiver offset is directly related to angle of incidence θ by the relationship (Sirgue and Pratt, 2004)

$$\cos\theta = \frac{z}{\sqrt{q^2+z^2}}, \tag{5}$$

where z is the depth of reflector, and q is the half the distance between the source and the receiver. Therefore, decomposing the objective function here is equivalent to a decomposition in the wavenumber domain based on the angles of incidence. For general media, the objective function is decomposed such that each term of the decomposed objective function has data that is sensitive to a limited area of the model's wavenumber spectrum $\delta\mathbf{m}$ using the diffraction terms (see Figure 2). With this direct mapping between terms in the decomposed objective function and the high-wavenumber components of the model, we can solve this system using Gauss-Seidel iterations, where the model at every iteration is updated using

$$\delta\mathbf{m}_i^h = \delta\mathbf{m}_i^{h-1} + \arg\min_{\mathbf{x}} \left\| \mathbf{W}_i^h \triangle\mathbf{d}_i^h \left(\mathbf{m}_i + \delta\mathbf{m}_i^{h-1} + \mathbf{x}\right) \right\|^2. \tag{6}$$

Here, we apply a few iterations of FWI with Gauss-Newton optimization for the model update $\mathbf{x}$ which is added to the initial model of the $i-$th stage $\mathbf{m}_i$ and the update from the previous Gauss-Seidel iteration $\delta\mathbf{m}_i^{h-1}$ to minimize the misfit function of the constant-offset data at the h-th offset. Note that low-wavenumbers components of the model, coupled by the tomographic terms, are freely updated during Gauss-Seidel iterations.

Due to the coupling, the low-wavenumber components of the model will oscillate between different passes through the Gauss-Seidel iterations. An under-relaxation scheme is used as a preconditioner to prevent this oscillatory behavior, where the under relaxation operator $\mathbf{S}_i$ is used during the update step between stages

$$\mathbf{m}_{i+1} = \mathbf{m}_i + \mathbf{S}_i\delta\mathbf{m}_i^N \tag{7}$$

where the $\mathbf{S}_i$ is a Gaussian smoothing operator applied to the cumulative update, the Gaussian smoothing filter is wide at early stages to allow updates to the very low-wavenumber components of the model, and the width of the filter is reduced gradually at later stages. We empirically find that smoothing along geological dip further accelerates the convergence process. Now, $\mathbf{m}_{i+1}$ is the initial model for the next stage of constant-offset inversions.

Figure 3 shows the corresponding FWI workflow. With each pass through the Gauss-Newton FWI block, a few iterations of FWI with the incomplete Gauss-Newton optimization (Akcelik et al., 2002; Erlangga and Herrmann, 2009; AlTheyab et al., 2013) are executed. The block in the workflow labeled *select uncycle-skipped data* designs the weighting operator $\mathbf{W}$ in equation 1, which masks the cycle-skipped data. The loop inside the area labeled *offset-rolling* minimizes the objective function using the Gauss-Seidel iterations.

SYNTHETIC AND FIELD DATA EXAMPLES

Now, we demonstrate the effectiveness of the proposed workflow on a synthetic data test. Data with 12 Hz peak-frequency

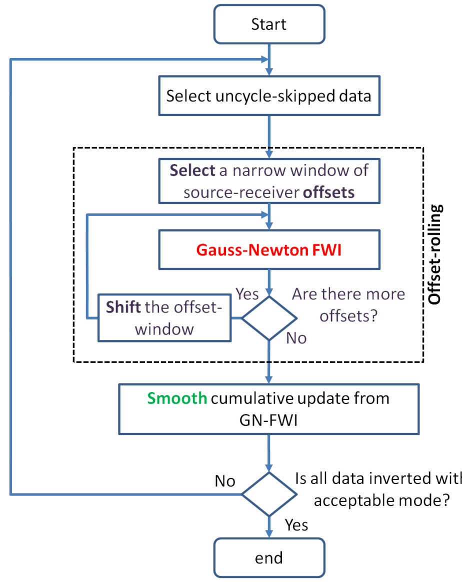

Figure 3: The proposed FWI workflow for inverting reflections with Gauss-Seidel iterations (offset-rolling).

and a 6 km maximum source-receiver offset were generated using the true model shown in Figure 4(a). The reweighted Gauss-Newton FWI (excluding cycle-skipped events) without the proposed workflow is applied to the synthetic data using the starting velocity model in Figure 4(b), which gives the results in Figure 4(c) after 300 iterations. The shallow part above 0.7 km is recovered mostly due to inverting diving waves. However, significantly more iterations are needed to recover the low-wavenumber components of the model in the deeper portions of the model. Moreover, the tomogram has many high-wavenumber artifacts that do not relate to any feature in the true model. On the other hand, using the proposed workflow gives the final tomogram in Figure 4(d) after 50 stages. The final tomogram is free from the high-wavenumber artifacts while maintaining the high-resolution of the shallow channels. In addition, the deeper fast layer at 1.5 km depth is positioned at the correct depth in the final tomogram.

Figure 5 depicts the results for inverting 2D GOM streamer data with a 4 km maximum offset and a 3-10 Hz frequency frequency range. To illustrate that the updates are are only inverted by the reflections, transmitted waves are muted. With a homogeneous starting velocity model of 2000 m/s the angle gathers have large moveout. The tomogram seen in Figure 5 is after 40 stages and the angle gathers are nearly flat indicating improvements to the velocity model.

CONCLUSIONS

We proposed a method for inverting reflections starting from inaccurate velocity models. At every stage, uncycle-skipped events are grouped according to a narrow-range of on source-receiver offsets, and the data from each offset are inverted sequentially, where the final model of a constant-offset FWI is the initial model for the next inversion at a wider source-

DOI http://dx.doi.org/10.1190/segam2015-5849854.1

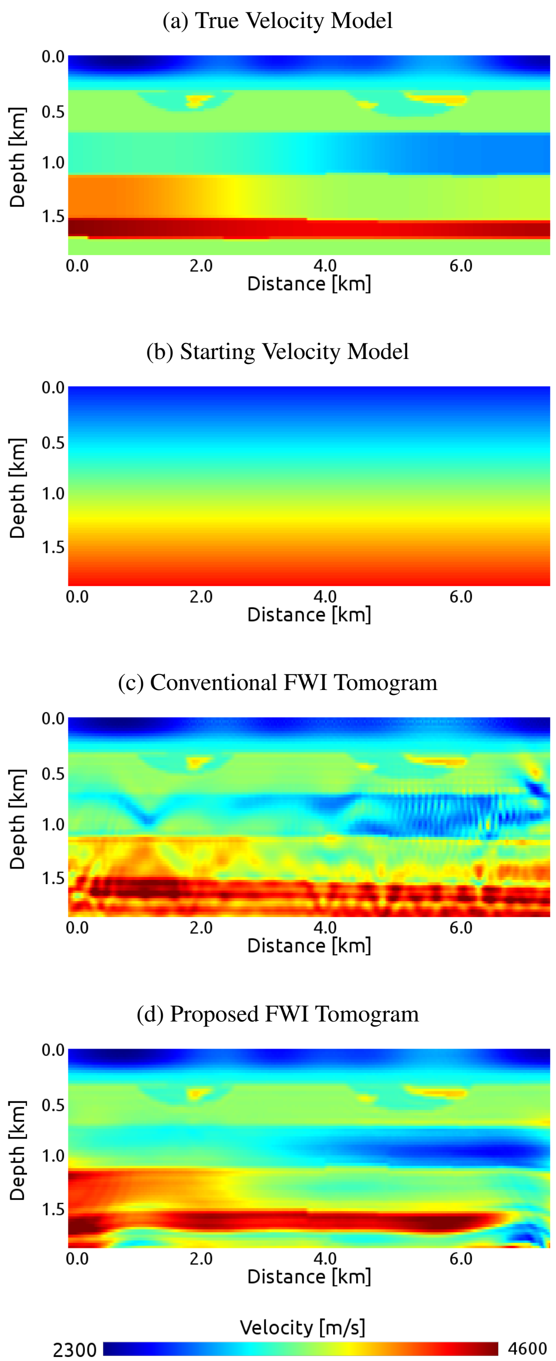

Figure 4: Conventional and proposed FWI applied to synthetic data.

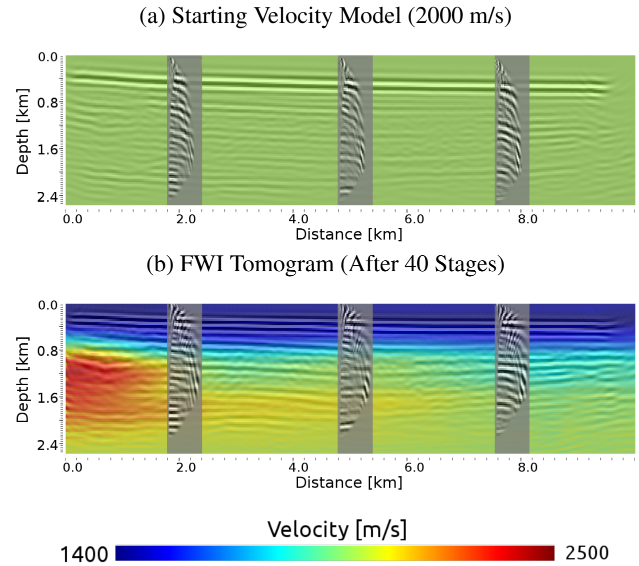

Figure 5: Proposed FWI applied to field data reflections. Reverse-time-migration images are overlaid onto the velocity models, and the three gray-scale panels are angle-domain common-image gathers.

receiver offset. Because of the direct mapping from offset to incidence angle in the wavenumber spectrum, this sequential inversion is related to Gauss-Seidel method. The constant offset formulation is applicable to layered media. Complex media might require an alternative formulation of Gauss-Seidel based on angle of incidence and/or frequencies. This will be the subject of a future research.

The Gauss-Seidel iterations have two advantages over the full-domain Newton inversion; it naturally enhances low-wavenumber updates, and it is easier to precondition with under-relaxation schemes. Here, we avoid the single scattering assumption and explicit scale separation, and the reflection data can still be inverted simultaneously with transmitted waves with Gauss-Seidel iteration, as shown in the synthetic data test. Our approach does not require generating common image gathers, which will be an advantage in 3D applications.

We observe that the method fails to invert strong multiples, post-critical reflections, and anisotropic effects in field data. We believe this is due to physics mismatch, where constant-density acoustic FWI is failing to explain the actual amplitude and waveform variations with offset. To alleviate problems with multiples, we prefer fast starting velocities which minimizes contributions of multiples to FWI updates.

ACKNOWLEDGMENTS

We thank the sponsors of the Center of Subsurface Imaging and Fluid Modeling consortium. AlTheyab thanks Saudi Aramco for sponsoring his studies at KAUST.

DOI http://dx.doi.org/10.1190/segam2015-5849854.1

EDITED REFERENCES

Note: This reference list is a copyedited version of the reference list submitted by the author. Reference lists for the 2015 SEG Technical Program Expanded Abstracts have been copyedited so that references provided with the online metadata for each paper will achieve a high degree of linking to cited sources that appear on the Web.

REFERENCES

Akcelik, V., G. Biros, and O. Ghattas, 2002, Parallel multiscale Gauss-Newton-Krylov methods for inverse wave propagation: Conference on Supercomputing, ACM/IEEE, Extended Abstracts, 41, doi:10.1109/SC.2002.10002.

AlTheyab, A., X. Wang, and G. Schuster, 2013, Time-domain incomplete Gauss-Newton full-waveform inversion of Gulf of Mexico data: 83rd Annual International Meeting, SEG, Expanded Abstracts, 5175–5179.

Asnaashari, A., R. Brossier, C. Castellanos, B. Dupuy, V. Etienne, Y. Gholami, G. Hu, L. Métivier, S. Operto, D. Pageot, V. Prieux, A. Ribodetti, A. Roques, and J. Virieux, 2012, Hierarchical approach of seismic full waveform inversion: Numerical Analysis and Applications, **5**, no. 2, 99–108, http://dx.doi.org/10.1134/S1995423912020012.

Bi, H., and T. Lin, 2014, Impact of adaptive data selection on full waveform inversion: 84th Annual International Meeting, SEG, Expanded Abstracts, 1094–1098.

Brossier, R., J. Virieux, and S. Operto, 2013, Toward data-domain waveform inversion of reflected waves: 83rd Annual International Meeting, Expanded Abstracts, 892–897.

Bunks, C., F. Saleck, S. Zaleski, and G. Chavent, 1995, Multiscale seismic waveform inversion: Geophysics, **60**, 1457–1473, http://dx.doi.org/10.1190/1.1443880.

Erlangga, Y. A., and F. J. Herrmann, 2009, Seismic waveform inversion with Gauss-Newton-Krylov method: 79th Annual International Meeting, SEG, Expanded Abstracts, 2357–2361.

Gauthier, O., J. Virieux, and A. Tarantola, 1986, Two-dimensional nonlinear inversion of seismic waveforms: Numerical results: Geophysics, **51**, 1387–1403, http://dx.doi.org/10.1190/1.1442188.

Gutiérrez, J. M., Á. A. Magreñán, and J. L. Varona, 2011, The "Gauss-Seidelization" of iterative methods for solving nonlinear equations in the complex plane: Applied Mathematics and Computation, **218**, 2467–2479, http://dx.doi.org/10.1016/j.amc.2011.07.061.

Mora, P., 1989, Inversion = migration tomography: Geophysics, **54**, 1575–1586, http://dx.doi.org/10.1190/1.1442625.

Sirgue, L., and R. G. Pratt, 2004, Efficient waveform inversion and imaging: A strategy for selecting temporal frequencies: Geophysics, **69**, 231–248, http://dx.doi.org/10.1190/1.1649391.

Tai, X.-C., 1992, Parallel function decomposition and space decomposition methods with applications to optimization, splitting and domain decomposition: Technical University Graz Technical Report 231.

Tarantola, A., 1984, Inversion of seismic reflection data in the acoustic approximation: Geophysics, **49**, 1259–1266, http://dx.doi.org/10.1190/1.1441754.

Virieux, J., and S. Operto, 2009, An overview of full-waveform inversion in exploration geophysics: Geophysics, **74**, no. 6, WCC1–WCC26, http://dx.doi.org/10.1190/1.3238367.

Wang, S., F. Chen, H. Zhang, and Y. Shen, 2013, Reflection-based full waveform inversion (RFWI) in the frequency domain: 83rd Annual International Meeting, SEG, Expanded Abstracts, 877–881.

DOI http://dx.doi.org/10.1190/segam2015-5849854.1

Xu, S., D. Wang, F. C. C. Zhang, and G. Lambaré, 2012, 74th Conference & Exhibition, EAGE, Extended Abstracts, W024.

Zhou, H., L. Amundsen, and G. Zhang, 2012, Fundamental issues in full waveform inversion: 82nd Annual International Meeting, SEG, Expanded Abstracts, doi:10.1190/segam2012-0878.1.

DOI http://dx.doi.org/10.1190/segam2015-5849854.1